# Analysis of experimental spectra of phosphine in the Tetradecad range near 2.3 $\mu$m using ab initio calculations

A.V. Nikitin, A. Campargue, A.E. Protasevich, K. Sung, Vl.G. Tyuterev, Michael M. Rey

# Analysis of experimental spectra of phosphine in the Tetradecad range near 2.3 μm using *ab initio* calculations

A.V. Nikitin[1], A. Campargue[2], A. E. Protasevich[1], M. Rey[3], K. Sung[4] , Vl. G. Tyuterev[1,3]

1. *Laboratory of Theoretical Spectroscopy, V.E. Zuev Institute of Atmospheric Optics, SB RAS, 1, Academician Zuev square, 634021, Tomsk, Russia*
2. *Univ. Grenoble Alpes, CNRS, LIPhy, 38000 Grenoble, France*
3. *Groupe de Spectrométrie Moléculaire et Atmosphérique, UMR CNRS 7331, Université de Reims, U.F.R. Sciences, B.P. 1039, 51687 Reims Cedex 2, France*
4. *Jet Propulsion Laboratory, California Institute of Technology, 4800 Oak Grove Drive, Pasadena, CA 91109, USA*

Number of Pages: 16
Number of Figures: 7
Number of Tables: 2
Number supplemental files 2

**Running Head:** Tetradecad spectrum of $PH_3$

**Keywords:** *infrared spectra, $AB_3$ molecules, line intensities, effective Hamiltonian, ab initio dipole, phosphine, Tetradecad, Jovian planets, Contact Transformations method.*

**Correspondence should be addressed to:**
Andrei V. Nikitin,
*Laboratory of Theoretical Spectroscopy, V.E. Zuev Institute of Atmospheric Optics, SB RAS, 1, Academician Zuev square, 634021, Tomsk, Russia
E-mail: avn@ iao.ru
Tel. +73822 - 491111-1208

**Abstract**

Due to its major interest for the chemistry of planetary atmospheres and exobiology, accurate spectroscopy data of phosphine are required for the search of signatures of this molecule in astronomical observations. In this work, high resolution infrared laboratory spectra of phosphine were analyzed for the first time in the full Tetradecad region (3769 - 4763 $cm^{-1}$) involving 26 rotationally resolved bands. Overall, 3242 lines were assigned in spectra previously recorded by Fourier transform spectroscopy at temperatures 200 K and 296 K, using a combined theoretical model based on *ab initio* calculations. The total nuclear motion Hamiltonian of $PH_3$ including *ab initio* potential energy surface, was reduced to an effective Hamiltonian using the high-order contact transformation method adapted to vibrational polyads of the $AB_3$ symmetric top molecules, followed by empirical optimization of the parameters. At this step, the experimental line positions were reproduced with a standard deviation of 0.0026 $cm^{-1}$ that provided unambiguous identification of observed transitions. The effective dipole transition moments of the bands were obtained by fitting to the intensities obtained from variational calculations using the *ab initio* dipole moment surface. The assigned lines were used to newly determine 1609 experimental vibration-rotational levels up to $J_{max}$= 18 with energy in the range 3896-6037 $cm^{-1}$ that represents significant extension towards higher energies compared to previous works. Transitions for all 26 sublevels of the Tetradecad were identified but with noticeably fewer transitions for fourfold excited bands because of their weaker intensity. At the final step, pressure-broadened half widths were attached to each transition and a composite line list adopting *ab initio* intensities and empirical line positions corrected to the accuracy of about 0.001 $cm^{-1}$ for strong and medium transitions was validated against experimental spectra available in the literature.

## 1. Introduction

Phosphine is a molecule of major interest for planetary atmospheres and exobiology. The search of its spectral signature in the microwave and infrared ranges has recently regained a strong attention in astronomical observation [***1***] [***2***] [***3***] [***4***] [***5***] [***6***] [***7***] [***8***] [***9***] [***10***] [***11***] [***12***]. It was found that phosphine is spectroscopically active and present in atmospheres of carbon stars [***1***] whereas some observed spectral features might be attributed to $PH_3$ also in brown dwarfs [***2***]. It was recently claimed [***4***] that $PH_3$ could represent a potential biosignature gas on anoxic (oxygen lacking) rocky planets or exoplanets. This is because on Earth, phosphine is associated with anaerobic ecosystems [***4***] [***13***] [***14***]. A particular role of phosphorus-bearing species in chemistry and biology was an incentive to find phosphine in the Venus atmosphere [***4***] [***5***] [***6***] [***7***] [***8***] [***9***] [***10***] [***11***] where an observation of $PH_3$ spectral signatures has become a controversial issue [***7***] [***8***] [***9***] [***10***] [***11***]. A surprising observation of phosphine in Venus using both the James Clerk Maxwell Telescope (JCMT) and the Atacama Large Millimeter Array (ALMA) facilities [***4***] [***5***] is yet to be confirmed [***6***] [***7***] [***8***] as no known process in the consensus model of atmosphere or geology could explain the presence of parts per billion $PH_3$ in Venus clouds [***15***]. Other hypotheses of phosphine anomalies as an extraordinary volcanism [***16***] [***17***] [***18***] or the biological explanation [***4***] [***15***] by analogy with biological production of $PH_3$ on Earth are under discussion. "If the presence of $PH_3$ in Venus' atmosphere is confirmed, it is highly likely to be the result of a process not previously considered plausible for Venusian conditions" [***19***]. Small concentrations (a few ppm) of phosphine occur in the atmospheres of Jupiter and Saturn [***20***] [***21***] [***22***] [***23***] [***24***]. In fact, $PH_3$ is expected to be well-mixed between the altitudes, yet the measurements for Saturn (*e.g.* at 0.5 bar sampled in the 10 μm range by Cassini/CIRS and at 2 - 3 bars in the 4.5 μm range by Cassini/VIMS) indicate a puzzling increase in their bulk abundance with altitude [***25***] As there are no known sources of $PH_3$ in the altitude range [***26***], such a finding is difficult to explain through atmospheric chemistry alone.

It seems to become a consensus in astrophysics, that other $PH_3$ spectral features should be sought [***4***], consequently an extension of accurate laboratory spectroscopy data of phosphine would be beneficial for further investigations in complementary spectral ranges. Note that recently developed methods using cross-correlation interpretation [***27***] [***28***] of astronomical observations require accurate high-resolution spectral data. Since the strongest bands (*e.g.* 4450 – 4650 $cm^{-1}$) corresponding to so called Tetradecad rovibrational upper states are located in the 2.2 μm region in the atmospheric window of the K band and they are fairly away from the strongest $CH_4$ bands (*e.g.* $\nu_1+\nu_4$ and $\nu_3+\nu_4$), the $PH_3$ Tetradecad bands

would be a good complementary region of interest for ground-based observations as well. These bands have not been assigned in laboratory experimental spectra because of the complexity in the rotationally resolved patterns. Corresponding line parameters are not yet available either in HITRAN [***29***], [***30***] GEISA [***31***] spectroscopic databases or *via* Virtual Atomic and Molecular Data Center (VAMDC) portal [***32***].

In this work, high resolution infrared laboratory spectra of phosphine recorded several decades ago at the National Solar Observatory on Kitt Peak in Arizona could be analyzed for the first time in the full Tetradecad region 3769 - 4763 $cm^{-1}$ involving 26 rotationally resolved bands using a theoretical model assisted with on *ab initio* calculations. The goal of the present work is to obtain an accurate theoretical modelling of these laboratory spectra in this range, to extent the knowledge of rovibrational levels towards higher energies and of line intensities for the corresponding transitions. In practical terms, we aim to provide an accurate and reliable line list for atmospheric remote sensing applications in the 2.3 µm region.

## 2. Theoretical background and an overview of previous works

Phosphine ($PH_3$) is a semi-rigid symmetric top molecule having four vibrational modes: two stretching non-degenerate modes $\nu_1(A_1)$ and $\nu_3(A_1)$ with frequency 2326.82 and 2321.14 $cm^{-1}$, respectively, and the two doubly degenerate bending modes, $\nu_2(E)$ and $\nu_4(E)$ with a frequency of 1118.31 $cm^{-1}$. Normal mode frequencies of $PH_3$ exhibit an approximate relation of stretching and bending frequencies, $\omega_1 \approx \omega_3 \approx 2\omega_2 \approx 2\omega_4$, resulting in vibrational levels being grouped into polyads. The vibrational energy levels with the same polyad number, $P = 2V_1 + V_2 + 2V_3 + V_4$, calculated from the four principal vibrational quantum numbers $V_i$ fall within the same energy range. The first polyads including ground vibrational state (GS), Dyad, Pentad, Octad and Tetradecad are presented on **Fig. 1**. In this work, we study the phosphine absorption spectra belonging to the Tetradecad band system that correspond to ($P$=0) $\rightarrow$ ($P$=4) bands.

Up to now, the four lower polyads up to the Octad ($P$=3) have been studied quite well and were included in the HITRAN [***33***] [***29***] and GEISA [***31***] databases. The HITRAN2020 database [***33***] includes a set of 104759 lines in the 0 - 3659.2657 $cm^{-1}$ range. Several bands in the $PH_3$ Octad were previously assigned [***34***] [***35***] [***36***] and theoretically modelled using an effective Hamiltonian and effective dipole transition moments. Recently, line positions and intensities of the Pentad bands (1500-2650 $cm^{-1}$) have also been revised [***37***]. In addition, theoretical studies [***38***] [***39***] [***40***] [***41***] have provided variational predictions of transitions obtained from *ab initio* potential energy surfaces (PES) and dipole moment surfaces (DMS)

[***42***] [***43***] [***40***]. Sousa-Silva et al. [***44***] applied the DMS of Ref. [***43***] to rotation-vibrational calculations of $PH_3$ spectra at $T$= 296 K [***44***] and at 1500 K [***45***] using the TROVE program [***46***]. Rey et al. [***47***] have calculated a theoretical list of lines at room temperature included in TheoReTS database and information system using the *ab initio* PES and DMS of Nikitin et al. [***39***] [***40***].

Formally, the definition of the phosphine polyads is similar to that of the methane polyads, though the resonance coupling interactions and the intensity distribution among the bands differ. The Tetradecad of phosphine consists of 14 vibrational bands divided into 26 vibrational sublevels, while in the case of methane there are 60 vibrational sublevels. Another difference is the localization of all two-quanta stretching vibration states at the top of the Tetradecad near 4600 $cm^{-1}$ above all three- and four-quanta vibration states (see **Fig. 1**) whereas the top of the methane Tetradecad is occupied by four-quanta states [***48***]. In the Tetradecad range, detailed analyses and theoretical modeling of high-resolution spectra of strongly coupled bands using purely empirical spectroscopic models become a complicated and tedious task. In case of methane, a full analysis of the Tetradecad bands has taken about fifteen years [***49***].

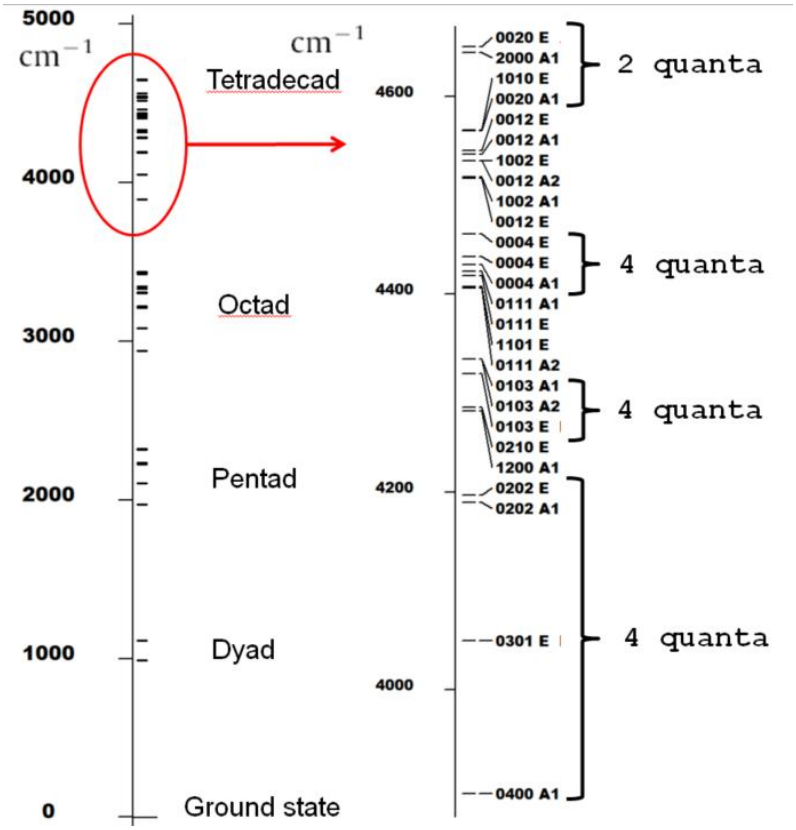


**Fig. 1.** *Vibrational levels of the $PH_3$ polyads (left side) and the vibrational sublevels of a part of Tetradecad (right side) corresponding to rovibrational bands analyzed in this work. The right hand side panel displays the principal vibration quantum numbers ($V_1V_2V_3V_4$), symmetry types of vibration sublevels. The symmetry types correspond to irreducible representations of the $C_{3v}$ point group.*

With the advent of accurate electronic structure calculations approaching the spectroscopic accuracy, this process can be efficiently assisted by first-principle predictions of rovibrational energy levels, line intensities and the interaction parameters of the polyad models. In the present work, we use a combined approach based on *ab initio* calculations with a subsequent empirical optimization.

To this end, we use the contact transformation (CT) method that permitted deriving initial effective Hamiltonians from an *ab initio* PES as described in [***50***], [***51***], [***48***], [***52***]. Another complementary method using numerical transformation of the Hamiltonian matrix with the application to $PH_3$ was suggested in [***53***]. In this work, we have built a CT effective Hamiltonian ($H^{eff}$) from the PES of Ref. [***39***] using a multi-step procedure. First, the full nuclear motion Hamiltonian of phosphine was reduced to an effective Hamiltonian using high-order CT method [***48***], [***52***] that included resonance coupling intra-polyad terms predicted from the *ab initio* PES. After that, this was expressed in the Irreducible Tensor Operators (ITO) formalism [***54***] [***55***] for a full account of symmetry properties for $AB_3$-type molecules, following the procedure described in [***56***]. At this step, the technique of the transformation is similar to that for methane previously considered in [***57***]. Typical accuracy of direct calculations of low-$J$ lines was within one wavenumber or even better, which allowed assigning a large part of the ro-vibrational patterns in the observed spectra. We proceeded then by a fine tuning of some $H^{eff}$ parameters, for which the variations were statistically well determined during the empirical optimization of the model. Since then, the number of assigned lines was iteratively increased whereas the RMS deviation for line positions dropped down to 0.002 - 0.003 $cm^{-1}$. This new CT-based effective Hamiltonian required less than half number of adjustable parameters with better predictive properties in comparison to purely empirical models [***36***].

The line intensities were computed in two steps.

First, variational calculations for line strengths were produced using our *ab initio* DMS of Ref. [***40***] in the normal-mode Eckart frame ITO representation according to the techniques described in [***47***]. This provided integrated intensities that agree with empirical values to about 2% for the Dyad and to 5-10% for the Pentad and Octad as discussed in [***40***]. A similar level of accuracy is achieved for strong lines. In cases of accidental resonances between nearby rovibrational states, the wavefunctions could be extremely sensitive to small errors in *ab initio* energy level calculations. Such small errors in energies may have a significant impact on the mixing coefficients of the wavefunction basis set expansions and thus produce erratic values in line strengths for the weaker transitions. This issue of “sensitive” (or

"unstable") line intensities in variational *ab initio* calculations is well-known for triatomic molecules [***58***] [***59***] and for larger molecules like methane [***60***]. A possible way to get rid of these erratic intensities of sensitive lines is a combined *ab initio*/effective model as discussed in [***48***], [***52***] for the methane polyads. Since the eigenvalues of the empirically optimized CT-based effective Hamiltonian match precisely experimental energy levels, the mixing of the basis set wavefunctions is also improved in the case of accidental resonances.

At the second step, we fit effective dipole transition moments of the bands to a subset of stable (non-perturbed by resonances) *ab initio* intensities produced by variational calculations and compute the entire set of transitions using the symmetry adapted MIRS code [***61***]. A comparison with experiment generally shows an improved agreement between theoretically simulated and experimental spectra.

## 3 Positions and Intensities Analysis in the Tetradecad Range

Since the 80's a number of FTS spectra of phosphine was recorded at the Kitt Peak National US Observatory spectra in the range 1579-5700 $cm^{-1}$ (see Table 1 of Butler et al. [***34***] and Table 1 of Ref. [***36***]). These spectra (including several low temperature scans at 210 K) were used to study the Octad region near 3 µm [***62***], but as illustrated on **Fig. 2**, strong Tetradecad bands are also clearly visible near 2.2 µm region. In the present work, an experimental list was retrieved from the room temperature Kitt Peak spectrum with reference number 840801R002 recorded with a spectral resolution of 0.0115 $cm^{-1}$. Line parameters of about 2000 lines with intensity above $5\times10^{-24}$ cm/molecule were retrieved using a multiline fitting program assuming a Voigt profile as line shape. As reliable values of the pressure and pathlength could not be obtained from the Kitt Peak archives files, absolute intensity values were obtained by scaling the fitted line areas. The scaling factor was obtained using the area of a ten of lines in the octad region measured in the same spectrum near 3400 $cm^{-1}$ for which absolute intensity values are provided in the HITRAN database [***30***]. In **Fig. 2**, the overview of the experimental stick spectrum is compared to the calculated spectrum. Note that the lines which appear to have experimental intensities largely overestimated compared to the calculated spectrum, are unresolved doublets which were considered as single line in the line profile fit.

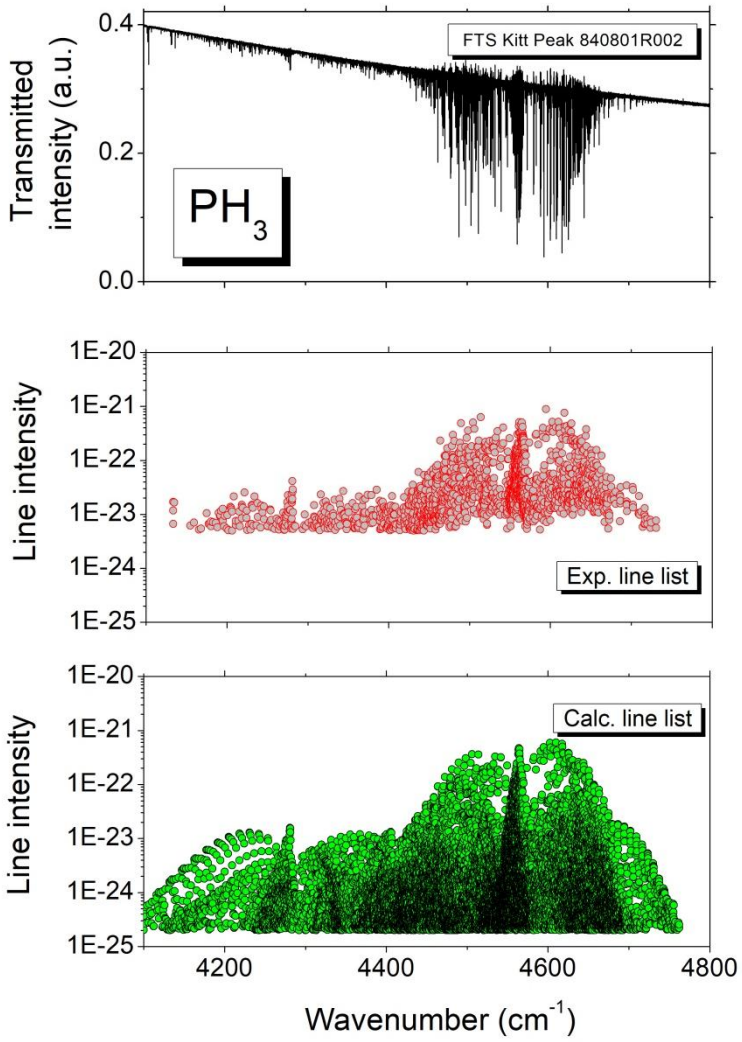


***Figure 2***

Upper panel: *The room temperature phosphine spectrum near 2.2 µm, recorded using the Kitt Peak FTS at 0.0115 cm$^{-1}$ resolution (Ref. 840801R002),*

Middle panel: *Experimental line list retrieved from the above FTS spectrum,*

Lower panel: *Tetradecad line list calculated in this work.*

*In the case of unresolved doublets, the experimental intensity values appear much larger than calculated.*

Contrary to the first four $PH_3$ polyads, which have been well modeled [***35***] [***34***] [***62***], previous identification of Tetradecad energy levels is very sparse. To our knowledge, it is limited to a few upper states of the $4\nu_2$-$\nu_2$ hot band transitions that fall in the Octad range. Maki et al. [***63***] reported 84 transitions for the $4\nu_2$-$\nu_2$ hot band, later Butler et al. [***34***] extended the number of the assignments to 125.

The modeling of the positions of the phosphine Tetradecad was noticeably simpler than that of the methane Tetradecad because of the smaller number of vibrational degrees of freedom. In addition, phosphorus has only one stable isotope, $^{31}P$, while natural methane

contains ~ 1% of $^{13}CH_4$. Together with the predictions using *ab initio* based calculations, this simplified the identification of the $PH_3$ spectra.

As discussed in the previous section, the cold Tetradecad bands were analyzed using an effective Hamiltonian constructed from the *ab initio* PES [***39***] by applying high-order contact transformations (CT) [***48***], [***52***] with a subsequent empirical optimization. First, the parameters specific to the lower polyads including the Octad [***62***] were slightly adjusted to line positions in the 1000-3600 $cm^{-1}$ range. This generally led to calculated low-*J* line positions of the Tetradecad bands down to an uncertainty of about 0.1 - 0.2 $cm^{-1}$, except for few outliers. Together with information on line intensities predicted from our *ab initio* DMS [***40***] using variational calculations [***47***], [***53***], this permitted assigning iteratively 3242 new $PH_3$ lines up to $J$= 18. The RMS of the (obs.-calc.) deviation for these line positions in the range 3896-4763 $cm^{-1}$ has quite rapidly converged to 0.0026 $cm^{-1}$ after a fine tuning of a subset of $H^{eff}$ parameters, whereas more than a half of parameters were held fixed to the values derived from the *ab initio* PES *via* the CT-method.

As mentioned in [***36***] [***62***] for $PH_3$ Octad, an accurate measurements and fitting of intensities is a complex and laborious task, because of many blended lines in the crowded spectra and because the partial pressure of this unstable molecule degraded in the cell during observations. The accuracy of empirically fitted intensities in the Dyad and Octad ranges has been evaluated as about 10-12%. Comparison of simulated theoretical spectra using *ab initio* intensities with the experimental ones showed a similar or even better agreement in their absorption coefficients, at least for strong and medium lines.

Therefore, we employed in this work a combined approach, in which the parameters of the effective dipole transitions moments (EDTM) of the Tetradecad bands were determined from *ab initio* line intensities computed by variational method [***40***], [***47***], [***53***]. As explained in Section 2, we used for the EDTM fit a subset of "stable" line intensities that are not strongly perturbed by sharp accidental resonances. The full set of line intensities was computed using this EDTM and accurate rovibrational eigenfunctions of the empirically optimized $H^{eff}$. The resulting calculated line list made it possible to identify transitions for all 24 vibrational bands in the observed spectra. The fit statistics are shown in **Table 1**. Overall, a sufficient number of assignments was obtained in the studied range, except for the weakest bands $3\nu_2+\nu_4$, $2\nu_2+2\nu_4$, $\nu_2+3\nu_4$ corresponding to four excited vibrational quanta. The EDTM parameters for the weak bands (all fourfold excited and some threefold excited vibrations) were fixed at zero since their absorption appeared to be mostly due to resonance intensity transfers from stronger bands. Note that the intensity distribution is quite different from that

of methane Tetradecad: the $2\nu_3$ (E) band of phosphine is weak, while for methane the $2\nu_3$ (E) and $2\nu_3$ ($F_2$) bands are the strongest bands.

**Table 1** Summary for the analyses of the Tetradecad $PH_3$ bands: line positions and intensity fit statistics.

| *Band* | *Band origin This Work* | *Band center* [***39***] | *Integrated Intensity (cmolecule)* | *#Positions* | *RMS* | *STD* | $J_{min}$ | $J_{max}$ | *#Intens* | *RMS* |
|---|---|---|---|---|---|---|---|---|---|---|
| $2\nu_1$ (A1) | 4644.6633 | 4646.50[a] | 2.8e-21 | 116 | 2.6 | 1.3 | 0 | 17 | 39 | 0.20 |
| $\nu_1+2\nu_2$ (A1) | 4282.4629 | 4283.96 | 1.1e-21 | 210 | 2.0 | 1.0 | 0 | 14 | 10 | 0.00 |
| $\nu_1+\nu_2+\nu_4$ (E) | 4407.7498 | 4408.36[b] | 9.5e-22 | 124 | 2.5 | 1.2 | 0 | 12 | 4 | 0.01 |
| $\nu_1+\nu_3$ (E) | 4565.8215 | 4566.98 | 5.8e-20 | 765 | 2.4 | 1.2 | 0 | 18 | 103 | 0.11 |
| $\nu_1+2\nu_2$ (E) | 4535.1834 | 4535.52 | 5.8e-21 | 203 | 2.5 | 1.2 | 1 | 15 | 33 | 0.10 |
| $\nu_1+2\nu_4$ (A1) | 4518.5996 | 4516.94 | 3.0e-21 | 167 | 2.3 | 1.1 | 1 | 16 | 26 | 0.04 |
| $4\nu_2$ (A1) | 3896.0154 | 3895.75 | 9.7e-23 | 52 | 2.6 | 1.3 | 0 | 10 | 0 | |
| $3\nu_2+\nu_4$ (E) | 4050.3521 | 4050.08 | 1.4e-23 | 3 | 6.3 | 3.1 | 4 | 8 | 0 | |
| $2\nu_2+\nu_3$ (E) | 4285.7254 | 4285.37 | 9.9e-22 | 338 | 2.0 | 1.0 | 0 | 14 | 0 | |
| $2\nu_2+2\nu_4$ (E) | 4197.0825 | 4196.57 | 1.7e-23 | 1 | 7.5 | 3.7 | 14 | 14 | 0 | |
| $2\nu_2+2\nu_4$ (A1) | 4189.7643 | 4189.36 | 4.7e-24 | 3 | 9.1 | 4.5 | 4 | 5 | 0 | |
| $\nu_2+\nu_3+\nu_4$ (A1) | 4423.1429 | 4422.59 | 1.4e-21 | 2 | 5.5 | 2.7 | 4 | 7 | 0 | |
| $\nu_2+\nu_3+\nu_4$ (A2) | 4406.4911 | 4406.08 | 3.6e-22 | 41 | 3.0 | 1.5 | 2 | 11 | 5 | 0.02 |
| $\nu_2+\nu_3+\nu_4$ (E) | 4419.2725 | 4419.50[b] | 1.6e-22 | 179 | 2.9 | 1.4 | 1 | 12 | 17 | 0.05 |
| $\nu_2+3\nu_4$ (A1) | 4335.0982 | 4334.15 | 1.4e-22 | 1 | 6.2 | 3.1 | 10 | 10 | 0 | |
| $\nu_2+3\nu_4$ (A2) | 4334.5040 | 4333.65 | 2.4e-23 | 1 | 2.9 | 1.4 | 9 | 9 | 0 | |
| $\nu_2+3\nu_4$ (E) | 4320.0009 | 4319.29 | 1.7e-23 | 12 | 4.6 | 2.3 | 1 | 10 | 0 | |
| $2\nu_3$ (E) | 4650.6412 | 4650.50 | 6.1e-22 | 10 | 6.7 | 3.3 | 5 | 11 | 0 | |
| $2\nu_3$ (A1) | 4565.5474 | 4566.86[a] | 1.9e-20 | 373 | 2.4 | 1.2 | 0 | 18 | 68 | 0.12 |
| $\nu_3+2\nu_4$ (A1) | 4541.5262 | 4541.11 | 5.3e-21 | 157 | 2.3 | 1.1 | 2 | 15 | 21 | 0.13 |
| $\nu_3+2\nu_4$ (E) | 4517.4739 | 4516.94 | 5.3e-21 | 209 | 2.9 | 1.4 | 1 | 15 | 22 | 0.05 |
| $\nu_3+2\nu_4$ (A2) | 4535.1144 | 4534.13 | 1.4e-21 | 44 | 2.9 | 1.4 | 3 | 13 | 7 | 0.04 |
| $\nu_3+2\nu_4$ (E) | 4545.3069 | 4544.58 | 4.2e-21 | 179 | 2.9 | 1.4 | 1 | 16 | 45 | 0.12 |
| $4\nu_4$ (E) | 4461.4004 | 4459.91 | 5.0e-22 | 33 | 2.6 | 1.3 | 7 | 12 | 0 | |
| $4\nu_4$ (E) | 4438.0193 | 4436.82 | 1.3e-21 | 13 | 4.6 | 2.3 | 7 | 17 | 0 | |
| $4\nu_4$ (A1) | 4430.3124 | 4429.20 | 3.4e-22 | 6 | 6.2 | 3.1 | 3 | 9 | 0 | |
| *All* | | | 1.13e-19 | 3242 | 2.6 | 1.4 | | | 400 | |

***Notes***
*The symmetry type of the upper vibration state is given in parentheses. RMS for line positions is given in units [0.001 $cm^{-1}$]; STD is dimensionless weighted standard deviation; RMS for line intensities is in %.* [a,b] *the corresponding upper vibrational states are strongly mixed. Integrated intensity corresponds to the sum of calculated line intensities of a band up to cut-off of* $2\times10^{-25}$ *cm/molecule.*

**Fig. 3** gives an example of experimental spectra and line assignments using the SpectraPlot program [***64***]. The two uppermost panels show the FTS spectra at 200 K and at room temperature [***34***], middle panel shows calculated spectra at 296 K with assignments in MIRS [***61***] format. The third and fourth panels shows the experimental list at 296 K and the calculated list at 296 K, respectively. **Fig. 4** gives an example of experimental spectra and line assignments in the range of $4\nu_2$, which is presented in the same format as in **Fig. 3** but with no

third panel. Traces of lines due to water (broadened by atmospheric air pressure) are noticeable at the right-hand side of **Fig .4**.

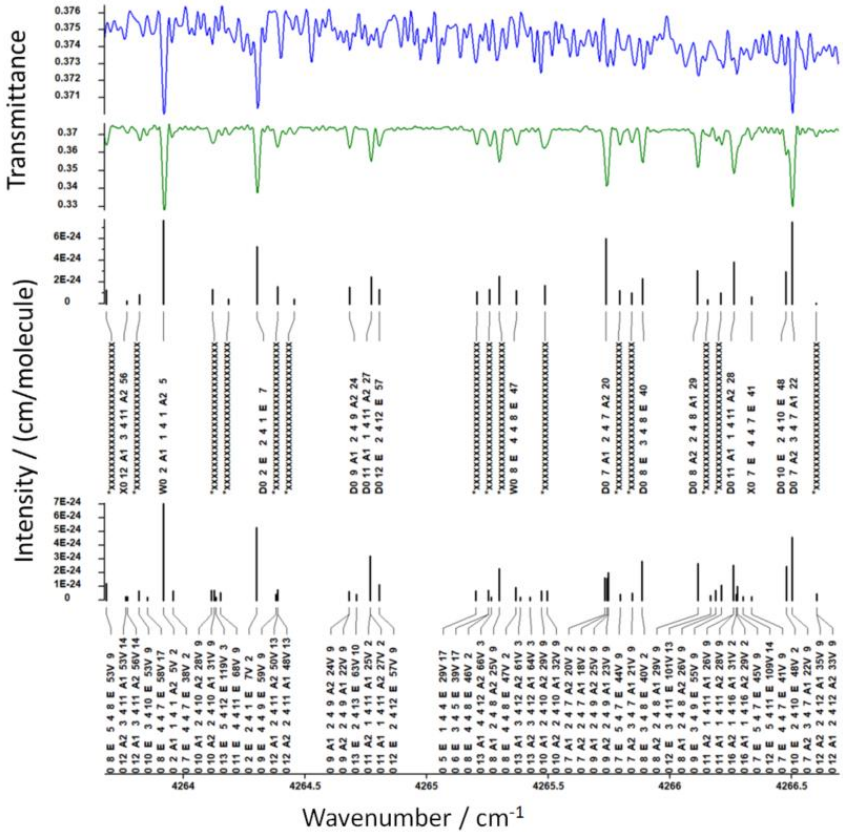


***Fig. 3.*** *Example of the $PH_3$ quantum assignment process using SpectraPlot program interface* [***64***]. *The upper panels show the FTS spectrum at 200 K (blue) and the second panel at room temperature* [***34***] *(green, 16.4 m optical path length). The third panel shows the sticks corresponding to the experimental line list at 296 K with assignments in MIRS* [***61***] *format. The fourth panel shows the sticks of our calculated lines at 296 K.*

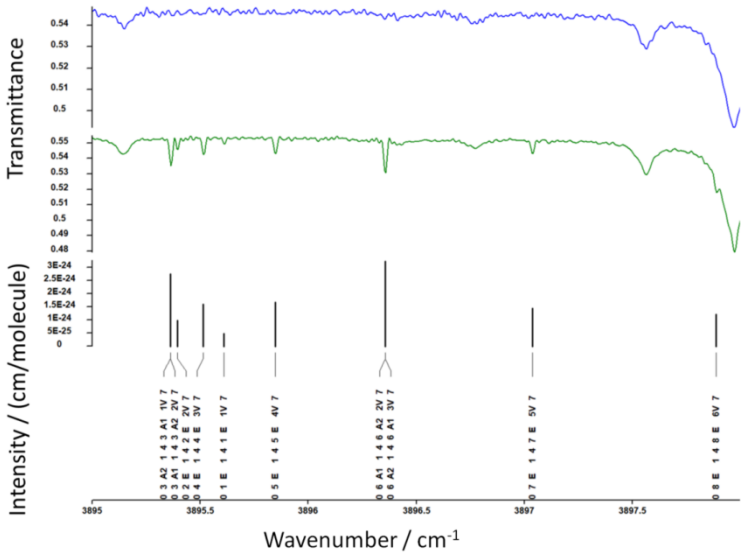


***Fig. 4.*** *Example of the $4v_2$ band quantum assignment. The upper panels show the FTS spectrum: the first panel at 200 K (blue) and the second panel at room temperature* [***34***] *(green, 16.4 m optical path length). The third panel shows the sticks of our calculated lines at 296 K.*

## 3. Vibration-rotation levels and resonance interactions among the Tetradecad states

The assigned lines were used to determine new 1609 experimental vibration-rotational levels up to $J_{max}$= 18 with energy in the range 3896-6037 $cm^{-1}$ that represents a significant extension towards higher energies compared to previous works. In total, the set of empirically determined levels includes 313, 462, and 834 levels of $A_1$, $A_2$ and E rovibrational symmetry types, respectively. The experimental energies per vibrational sublevels are provided as a Supplementary Material file which includes the ro-vibrational assignment and three major contributions of the basis set function for each state. The assignment is given according to the first major coefficient of the expansion of the final wavefunctions in the rotation-vibration basis set. In some cases, the second and the third expansion coefficients have values comparable with the first one. This results from the quite strong and irregular couplings due to resonance interactions within the Tetradecad. An example of the variation of the absolute value of the second coefficient in the wavefunction expansion is plotted in **Fig. 5** between $V_1V_2V_3V_4$ ($\Gamma_v$) = 1010 (E) and 0020 (E) sublevels *versus* energy.

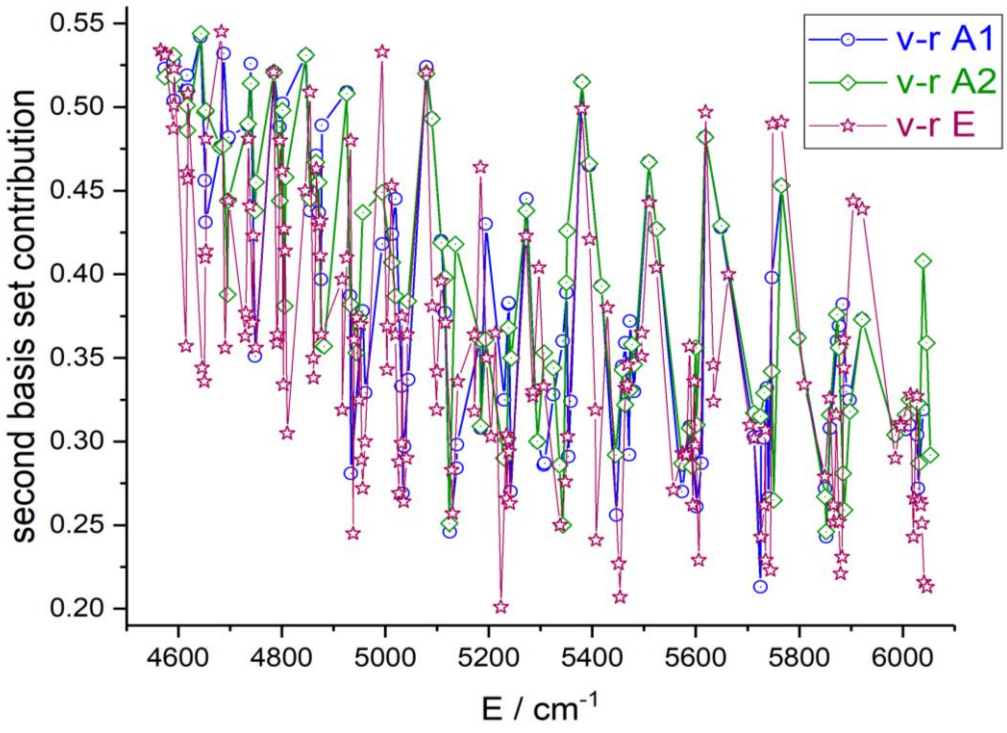


**Figure 5.** *An example of the irregular behavior of the wavefunction coupling coefficients (absolute value of the second coefficient in the expansion in the basis set functions) between rovibrational states of $V_1V_2V_3V_4$ ($\Gamma_v$) = 1010 (E) and 0020 (E) sublevel versus rovibrational energy (upper panel) and the upper J value (lower pane): see the Supplementary Materials for more detailed information. Blue curve corresponds to A1-type, green curve to A2-type and red curve to E-type vibration-rotation levels.*

## 4. Combined line list for line positions and intensities

The line list for the Tetradecad transitions was constructed in two steps. First, the line positions and line intensities were computed using empirically optimized $H^{eff}$ and the dipole transition moments of all bands fitted to "stable" *ab initio* intensities with the MIRS code [***61***]. The intensity cut-off was fixed to $2\times10^{-25}$ cm/molecule. At this step, the RMS (obs.-calc.) deviation of the line position fit was 0.0026 $cm^{-1}$ for 3242 transitions. The average intensity uncertainty for strong lines is estimated as 5% by comparison of the simulated and observed spectra. At the second step, for all identified transitions, the calculated positions were replaced by the experimental ones. In addition, the positions of unassigned calculated transitions reaching determined upper state levels $E_{upper}$ were replaced by ($E_{upper} - E_{lower}$). This makes the line position accuracy to be about 0.001 $cm^{-1}$ or better for the most of strong and medium lines in the final list. The calculated list at 296 K including the assignments from the present work is provided as Supplementary Material. A typical example of agreement for line positions and intensities and experimental Kitt Peak spectrum in a blown up scale is given in **Fig. 6**.

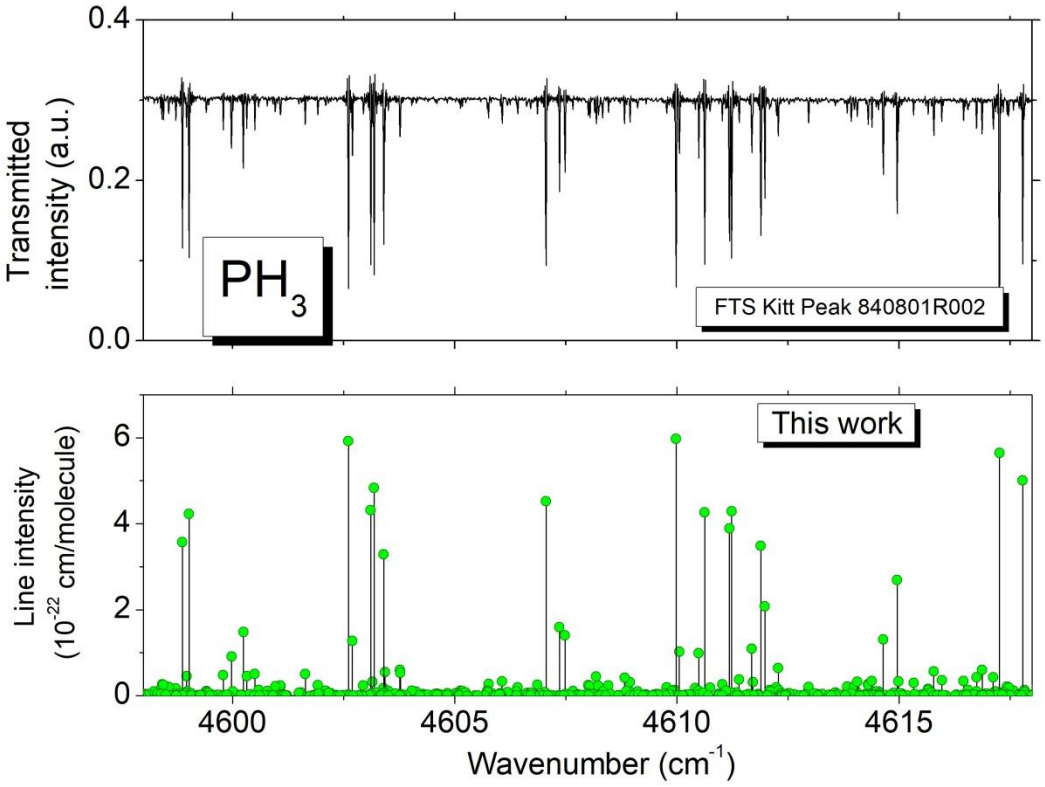


**Figure 6.** *An example of an agreement for line positions and intensities between our line list and a room temperature Kitt Peak spectrum (Ref. 840801R002).*

A sample of the list is given in **Table 2**; this includes the rovibrational quantum assignments (the assignment notation is described in the notes of Table 3 of ref. [***62***]) and the lower state energies.

**Table 2.**
An excerpt of Electronic Supplementary data: spectroscopic line parameters of $PH_3$ at 296 K with assignment in the 3769-4763 $cm^{-1}$ region.

| Iso* | ν($cm^{-1}$)[a] | Int. (296 K)[b] cm/molec. | self HW[c] | air HW[d] | $E_{low}$ $cm^{-1}$ [e] | $n$ [f] | Rotational assignment[g] | | Vibr. state[h] |
|---|---|---|---|---|---|---|---|---|---|
| | | | | | | | *Upper state* | *Lower state* | |
| 281 | 4349.03464 | 2.276E-25 | 0.072 | 0.104 | 386.6223 | .61 | 4 8 7 E 112 | 0 9 5 E 3 | 0111A1 |
| 281 | 4349.15310 | 3.794E-25 | 0.063 | 0.094 | 787.7732 | .57 | 4 14 6 A1 41 | 0 13 6 A2 3 | 1200A1 |
| 281 | 4349.15646 | 3.800E-25 | 0.063 | 0.094 | 787.7732 | .57 | 4 14 6 A2 39 | 0 13 6 A1 3 | 1200A1 |
| 281 | 4349.16780 | 5.379E-25 | 0.068 | 0.098 | 566.8762 | .59 | 4 12 7 A1 35 | 0 11 6 A2 2 | 0210E |
| 281 | 4349.16786 | 5.379E-25 | 0.068 | 0.098 | 566.8762 | .59 | 4 12 7 A2 33 | 0 11 6 A1 2 | 0210E |
| 281 | 4349.22787 | 2.576E-24 | 0.053 | 0.091 | 628.0441 | .58 | 4 11 10 E 135 | 0 12 11 E 1 | 0111E |
| 281 | 4349.36179 | 4.439E-24 | 0.080 | 0.112 | 184.6638 | .64 | 4 5 1 E 58 | 0 6 2 E 3 | 1101E |
| 281 | 4349.42990 | 2.472E-24 | 0.077 | 0.102 | 294.0276 | .62 | 4 9 8 E 45 | 0 8 7 E 2 | 0210E |
| 281 | 4349.64044 | 3.834E-25 | 0.067 | 0.104 | 580.8453 | .59 | 4 10 3 A1 77 | 0 11 3 A2 3 | 0004A1 |
| 281 | 4349.73405 | 5.822E-25 | 0.084 | 0.112 | 128.6891 | .65 | 4 4 4 A2 19 | 0 5 3 A1 1 | 0111E |
| 281 | 4349.73412 | 5.823E-25 | 0.084 | 0.112 | 128.6890 | .65 | 4 4 4 A1 22 | 0 5 3 A2 1 | 0111E |
| 281 | 4349.75651 | 2.068E-25 | 0.059 | 0.091 | 911.2002 | .56 | 4 15 6 A2 45 | 0 14 6 A1 3 | 1200A1 |
| 281 | 4349.75904 | 2.074E-25 | 0.059 | 0.091 | 911.2002 | .56 | 4 15 6 A1 43 | 0 14 6 A2 3 | 1200A1 |

*Notes:*
** Molecule and Isotopologue number in the HITRAN notation, i.e. 281 for $^{31}PH_3$*
[a] *calculated line positions*
[b] *calculated line intensity at 296 K*
[c] *Self-broadening coefficient in $cm^{-1}$/atm (See Sec.3 for details)*
[d] *Air-broadening coefficient in $cm^{-1}$/atm (See Sec.3 for details)*
[e] *Lower state energy in $cm^{-1}$*
[f] *temperature dependence exponent of the air-broadening coefficient*
[g] *Lower and upper state rovibrational assignments are given by the vibrational polyad number P, the rotational quantum number J, the rovibrational symmetry type C ($C_{3v}$ irreducible representation) and the ro-vibration ranking index α* [***61***]
[h] *Upper vibrational state*

## 5. Insertion of pressure-broadened half widths and validation tests under atmospheric conditions

Devi et al. [***37***] reported that no significant vibrational dependence of the self-widths was observed between the Pentad ($2\nu_4$, $\nu_1$, $\nu_3$) and Dyad ($\nu_2$, $\nu_4$) regions for the transitions having identical rotational quantum numbers. Thus, we have introduced self- and $N_2$-broadened half-widths in this Tetradecad region following the same procedure as in the Octad region [***62***]. Briefly, for self-widths, we have borrowed the self-width values measured for the $\nu_3$ band by Devi et al. [***37***], by matching their quantum identifiers ($J$, $K$, $\Delta J$, and $\Delta K$). For the transitions having no match in their quantum assignments, their median values over $K$ are adopted for the given $J$. For $N_2$-broadening, we have adopted the measurements of Bouanich et al. [***65***] in the Dyad region. Either case, for the transitions with $J \geq 18$, a default value of 0.05 and 0.08 $cm^{-1}$/atm was assumed, respectively. For the temperature dependence exponents

of the $N_2$-broadening coefficients, we have assumed a $(0.72 - 0.01J)$ rotational dependence based on the work of [***66***] as was suggested by Butler et al. [***34***].

As part of a sanity check of the resulting line list, a synthetic spectrum based on the PNNL cross sections [***67***] [***68***] was calculated for 50 Torr of $PH_3$ diluted in 710 Torr of nitrogen at 25°C and compared with a spectrum generated with our line list. As presented in **Fig. 7**, the residuals are at the noise level (about 1% of the transmittance) across the spectral region, showing the good quality of the line list from the present work.

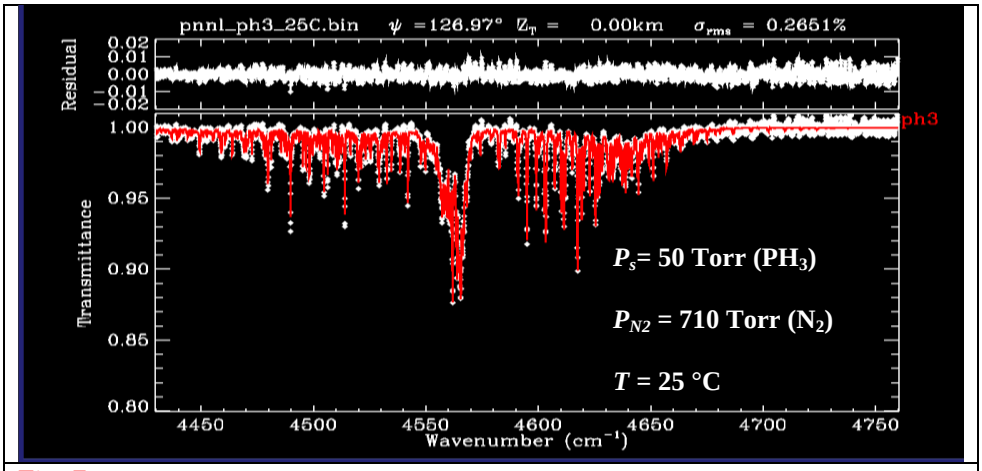


Fig. 7
*Comparison of the PNNL-cross section based spectrum (white) and a synthetic spectrum (red) generated with the current line list, showing their differences less than 1 % in the upper trace.*

A more detailed "mirror-type" comparison is presented in **Fig. 8** for the upper part of the Tetradecad. This provides an independent confirmation of the high accuracy of the line list both in terms of line positions, intensities and line widths under atmospheric conditions. The line list can be useful for the next editions of the HITRAN [***30***] [***29***] and GEISA [***31***] databases.

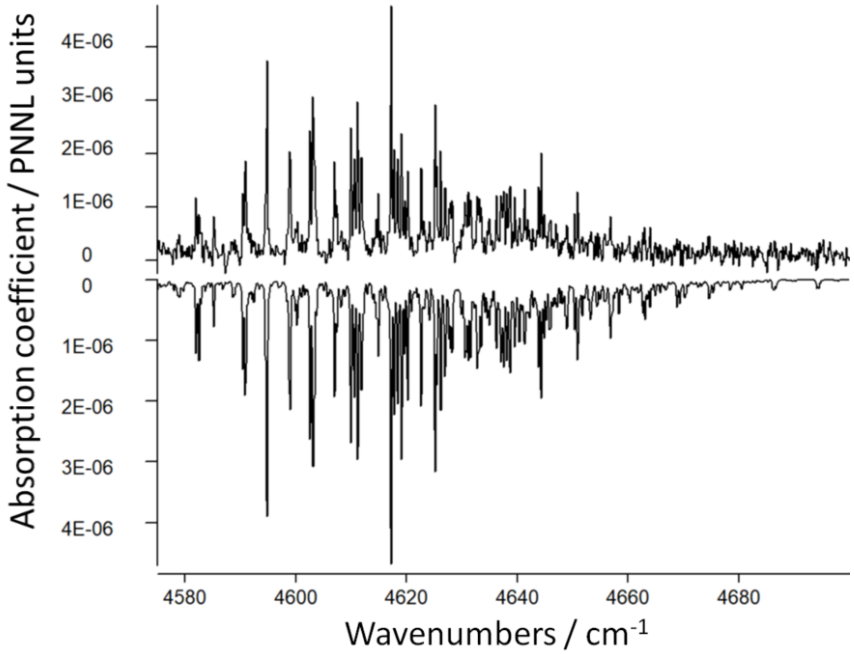


**Fig. 8**

*Comparison of the PNNL absorption coefficients derived at 25°C* [***69***] *(upper pane) with the calculated values (lower pane) based on this work in the 4575-4700 cm$^{-1}$ region.*

## 6. Concluding remarks

So far, only global variational lists of ExoMol [***45***] and TheoReTS [***47***] lines have been available in the Tetradecad range of phosphine spectrum. The accuracy of line positions in such calculations is limited mainly by the accuracy of the PESs supporting vibration-rotation levels and also by the convergence of the variational methods linked to necessary truncation of infinite-dimensional Hamiltonian matrices. The first analysis of high resolution experimental phosphine spectra using combined (*ab initio*/$H^{eff}$) model carried out in this work has permitted improving the accuracy of line positions by two or three orders of magnitude for the cold bands in the Tetradecad range.

A good agreement of *ab initio* intensities both with high-resolution Kitt Peak and medium resolution PNNL spectra provides a validation of the dipole moment surface [***40***], which was used in the calculations. The set of new 1609 Tetradecad levels deduced from experimental spectra extends the knowledge of vibration-rotation states towards higher energies in the range 3896-6037 cm$^{-1}$. This will be useful for future assignments of high-temperature spectra in conditions typical for many astronomical observations.

**Acknowledgements**

Support from the ANR-RNF TEMMEX project (grants ANR-21-30CE-0053-01 and RNF 22-42-09022) is acknowledged. Part of the research was performed at the Jet Propulsion Laboratory (JPL), California Institute of Technology under contracts with the National Aeronautics and Space Administration. The support of the CNRS (France) in the frame of International Research Project SAMIA is acknowledged.

## References


[1] Agundez M., Cernicharo J., Decin L., Encrenaz P., Teyssier D., Confirmation of circumstellar phosphine. *Astrophys J. Lett* 2011;790: L27.

[2] Sousa-Silva C., Seager S., Ranjan S., Petkowski J.J., Zhan Z., Hu R., Bains W., Phosphine as a Biosignature Gas in Exoplanet Atmospheres. *Astrobiology* 2020;20: 235–268.

[3] Dransfield G. , Triaud A., Colour–magnitude diagrams of transiting exoplanets – III. A public code, nine strange planets, and the role of phosphine *NMRAS* 2020;499: 505–519.

[4] Greaves J.S., Richards A.M.S., Bains W., Rimmer P.B., Sagawa H., Clements D.L., Seager S., Petkowski J.J., Sousa-Silva C., Ranjan S., al. et, Phosphine gas in the cloud decks of Venus. *Nature Astron.* 2021;5: 655–664.

[5] Greaves J.S., Richards A.M.S., Bains W., Rimmer P.B., Sagawa H., Clements D.L., Seager S., Petkowski J.J., Sousa-Silva C., Ranjan S., al. et, Addendum: Phosphine gas in the cloud deck of Venus. *Nature Astron.* 2021;5: 726–728.

[6] Encrenaz T., Greathouse T.K., Marcq E., Widemann T., Bézard B., Fouchet T., Giles R., Sagawa H., Greaves J., Sousa-Silva C., A stringent upper limit of the PH3 abundance at the cloud top of Venus. *Astron. Astrophys.* 2020;643: L5.

[7] Villanueva G., Cordiner M., Irwin P., de Pater I., Butler B., Gurwell M., Milam S., Nixon C., Luszcz-Cook S., Wilson C., al. et, No evidence of phosphine in the atmosphere of Venus from independent analyses. *Nature Astron.* 2021;5: 631–635.

[8] Greaves J.S., Richards A.M.S., Bains W., Rimmer P.B., Clements D.L., Seager S., Petkowski J.J., Sousa-Silva C., Ranjan S., Fraser H.J., Reply to: No evidence of phosphine in the atmosphere of Venus from independent analyses. *Nature Astron.* 2021;5: 636–639.

[9] Trompet L., Robert S., Mahieux A., Schmidt F., Erwin J., Vandaele A.C., Phosphine in Venus' atmosphere: Detection attempts and upper limits above the cloud top assessed from the SOIR/VEx spectra. *Astron. Astrophys.* 2021;645: L4.

[10] Cordiner M., Villanueva G., Wiesemeyer H., Milam S., de Pater I., Moullet A., Aladro R., Nixon C., Thelen A., Charnley S., al. et, Phosphine in the Venusian Atmosphere: A Strict Upper Limit from SOFIA GREAT Observations. *Geophys. Res. Lett.* 2022;49: e2022GL101055.

[11] Lincowski A.P., Meadows V.S., Crisp D., Akins A.B., Schwieterman E.W., Arney G.N., Wong M.L., Steffes P.G., Parenteau M.N., Domagal-Goldman S., Claimed Detection of PH3 in the Clouds of Venus Is Consistent with Mesospheric SO2. *Astrophys. J. Lett.* 2021;908: L44.

[12] Omran A., Oze C., Jackson B., Mehta C., Barge L.M., Bada J., Pasek M.A., Phosphine Generation Pathways on Rocky Planets. *Astrobiology* 2021;21: 1264–1276.

[13] Devai I., Felfoldy L., Wittner I., Plosz S., Detection of phosphine: new aspects of the phosphorus cycle in the hydrosphere. *Nature* 1988;333: 343–345.

[14] Jenkins R.O., Morris T.-A., Craig P.J., Ritchie A.W., Ostah N., Phosphine generation by mixed and monoseptic cultures of anaerobic bacteria. *Sci Total Environ* 2000;250: 73-81.

[15] Cleland C.E. , Rimmer P.B., Ammonia and Phosphine in the Clouds of Venus as Potentially Biological Anomalies. *Aerospace* 2022;9: 752.

[16] Bains W., Petkowski J.J., Seager S., Ranjan S., Sousa-Silva C., Rimmer P.B., Zhan Z., Greaves J.S., Richards A.M.S., Phosphine on Venus Cannot Be Explained by Conventional Processes. *Astrobiology* 2021;21: 1277–1304.

[17] phosphine. Volcanicallyextruded phosphides as an abiotic source of Venusian, *Proc. Natl. Acad. Sci. USA* 2021;118: e2021689118.

[18] Bains W., Shorttle O., Ranjan S., Rimmer P.B., Petkowski J.J., Greaves J.S., Seager S., Only extraordinary volcanism can explain the presence of parts per billion phosphine on Venus. *Proc. Natl. Acad. Sci. USA* 2022;119: e2121702119.

[19] Bains W., Petkowski J., Seager S., Ranjan S., Sousa-Silva C., al et, Venusian phosphine: a 'wow!' signal in chemistry? *Phosphorus, Sulfur, and Silicon and the Related Elements* 2022;197, no. 5-6: 438-443.

[20] Kunde V., Hanel R., Maguire W., Baluteau J.P., Marten A., Chedin A., Husson N., Scott N., The tropospheric gas composition of Jupiter's north equatorial belt /NH3, PH3, CH3D, GeH4, H2O/ and the Jovian D/H isotopic ratio *Atrophys. J* 1982;263: 443-467.

[21] Chedin A. , Scott N.A., The impact of spectroscopic parameters on the composition of the jovian atmosphere discussed in connection with recent laboratory, earth and planetary observation programs *J. Quant. Spectrosc. Radiat. Transfer.* 1984;32: 463-477.

[22] Fletcher L.N., Orton G.S., Teanby N.A., Irwin P.G.J., Phosphine on Jupiter and Saturn from Cassini/CIRS *Icarus* 2009;202: 543-564.

[23] Drossart P., Lellouch E., Bézard B., Maillard J.-P., Tarrago G., Jupiter - Evidence for phosphine enhancement at high northern latitudes *Icarus* 1990;83: 248-253.

[24] Larson H.P., Fink U., Smith H.A., Davis D.S., The middle-infrared spectrum of Saturn: Evidence for phosphine and upper limits to other trace atmospheric constituents *Astrophys. J.* 1980;240: 327–337.

[25] Fletcher L.N., Baines K.H., Momary T.W., Showman A.P., Irwin P.G.J., Orton G.S., Roos-Serote M., Merlet C., *Icarus* 2011;214: 510–533.

[26] Fegley B.J. , Lodders K., Chemical models of the deep atmospheres of Jupiter and Saturn *Icarus* 1994;110: 117-154.

[27] Snellen I.A.G., Brandl, B. R., de Kok, R. J., et al., Fast spin of the young extrasolar planet β Pictoris b *Nature* 2014;509: 63.

[28] de Regt S., Kesseli A.Y., Snellen I.A. G., R. MerrittS., L. ChubbK., A quantitative assessment of the VO line list: Inaccuracies hamper high-resolution VO detections in exoplanet atmospheres *A&A* 2022;661: A109.

[29] Rothman L.S., Gordon I.E., Babikov Y., Barbe A., Chris Benner D., Bernath P.F., The HITRAN2012 molecular spectroscopic database. *J. Quant. Spectrosc. Radiat. Transfer* 2013;130: 4-50.

[30] Gordon I.E., Rothman L.S., Hill C., Kochanov R.V., Tan Y., Bernath P.F., al. et, The HITRAN2016 molecular spectroscopic database. *J Quant Spectrosc Radiat Transfer* 2017;203: 3-69.

[31] Delahaye T., Armante R., Scott N.A., al. et, The 2020 edition of the GEISA spectroscopic database *Journal of Molecular Spectroscopy* 2021;380: 111510.

[32] Albert D., Antony B.K., Ba etal., A decade with VAMDC: Results and ambitions *Atoms*;8: 76.

[33] Gordon I.E., Rothman L.S., Hargreaves R.J., Hashemi R., Karlovets E.V., Skinner F.M., al et, The HITRAN2020 molecular spectroscopic database *J. Quant. Spectrosc. Radiat. Transfer*. 2022;277: 107949.

[34] Butler R.A.H., Sagui L., Kleiner I., Brown L.R., The absorption spectrum of phosphine (PH3) between 2.8 and 3.7 lm: Line positions, intensities, and assignments *J. Molec. Spectrosc.* 2006;238: 178–192.

[35] Ulenikov O.N., Bekhterevaa E.S., Kozinskaiaa V.A., Zheng J.-J., Heb S.-G., Hub S.-M., Zhub Q.-S., Leroy C., Pluchart L., High-resolution spectrum of the v1 + v4(E); v3 + v4(E); v3 + v4(A1), and v3 + v4(A2) bands of the PH3 molecule: assignments and preliminary analysis *J. Quant. Spectrosc. Radiat. Transfer* 2004;83: 599-618.

[36] Nikitin A.V., Champion J.-P., Butler R.A.H., Brown L.R., Kleiner I., Global modeling of the lower three polyads of PH3: Preliminary results *J. Molec. Spectrosc* 2009;256: 4-16.

[37] Malathy Devi V., Kleiner I., Sams R.L., Brown L.R., Benner D.C., Fletcher L.N., Line Positions and Intensities of the Phosphine (PH3) Pentad near 4.5 μm *J. Molec. Spectrosc.* 2014 2014;298: 11–23.

[38] Ovsyannikov R., Yurchenko S.N., Carvajal M., Thiel W., Jensen P., Vibrational energies of PH3 calculated variationally at the complete basis set limit *J. Chem. Phys.* 2008;129: 044309.

[39] Nikitin A.V., Holka F., Tyuterev Vl.G., Fremont J., Vibration energy levels of the PH3, PH2D, and PHD2 molecules calculated from high order potential energy surface *J. Chem. Phys* 2009;131: 244312.

[40] Nikitin A.V., Rey M., Tyuterev Vl.G, High order dipole moment surfaces of PH3 and ab initio intensity predictions in the Octad range *J. Molec. Spectrosc* 2014;305: 40-47.

[41] Sousa-Silva C., Tennyson J., Yurchenko S.N., Communication: Tunnelling splitting in the phosphine molecule *Journal of Chemical Physics* 2016;145, no. 9: 091102.

[42] He S.G., Zheng J.J., Hu S.M., Lin H., Ding Y., Wang X.H., Zhu Q.S., The stretching vibrational overtone spectra of PH3: Local mode vibrational analysis, dipole moment surfaces from density functional theory and band intensities *J. Chem. Phys* 2001;114: 7018-7026.

[43] Yurchenko S.N., Carvajal M., Thiel W, Jensen P., Ab initio dipole moment and theoretical rovibrational intensities in the electronic ground state of PH3 *J. Molec. Spectrosc.* 2006;239: 71-87.

[44] Sousa-Silva C., Yurchenko S.N., Tennison J, A computed room temperature line list for phosphine *J. Molec. Spectrosc.* 2013;288: 28-36.

[45] Sousa-Silva C., Al-Refaie A.F., Tennyson J., Yurchenko S.N., Exomol line lists - VII. the rotation-vibration spectrum of phosphine up to 1500 K *Monthly Notices of the Royal Astronomical Society* 2015;446, no. 3: 2337-2347.

[46] Yurchenko S.N., Thiel W., Jensen P., Theoretical rovibrational energies (trove): A robust numerical approach to the calculation of rovibrational energies for polyatomic molecules. *J. Mol. Spectrosc.* 2007;245: 126-140.

[47] Rey M., Nikitin A.V., Babikov Y., Tyuterev Vl.G., TheoReTS – An information system for theoretical spectra based on variational predictions from molecular potential energy and dipole moment surfaces *J. Molec. Spectrosc.* 2016;327: 138–158.

[48] Tyuterev Vl.G., Tashkun S.A., Rey M., Kochanov R.V., Nikitin A.V., Delahaye T., Accurate spectroscopic models for methane polyads derived from a potential energy surface using high-order contact transformations. *The Journal of Physical Chemistry* 2013;117: 13779−13805.

[49] Nikitin A.V., Chizhmakova I.S., Rey M., Tashkun S.A., Kassi S., Mondelain D., Campargue A., Tyuterev Vl.G., Analysis of the absorption spectrum of 12CH4 in the region 5855-6250 cm-1 of the 2v3 band *J. Quant. Spectrosc. Radiat. Transfer.* 2017: https://doi.org/10.1016/j.jqsrt.2017.05.014.

[50] Tyuterev VI.G., Tashkun S.A., Rey M., Kochanov R.V., Nikitin A.V., Delahaye T., Accurate spectroscopic models for methane polyads derived from a poten- tial energy surface using high-order contact transformations *J. Phys. Chem.* 2013;117: 13779–805.

[51] Tyuterev Vl.G., Tashkun S.A., Seghir H., "High-order contact transformations: general algorithm, computer implementation, and triatomic tests," *SPIE*, vol. 5311, pp. 164 - 176, 2004.

[52] Tyuterev V.G., Tashkun S., Rey M, Nikitin A., High-order contact transformations of molecular Hamiltonians: general approach, fast computational algorithm and convergence of ro-vibrational polyad models *Molec. Phys.* 2022;120: e2096140.

[53] Rey M, Novel methodology for systematically constructing global effective models from ab initio-based surfaces: A new insight into high-resolution molecular spectra analysis *J. Chem. Phys* 2022;292: 108349.

[54] Champion J.-P., Loete M., Pierre G., *Spectroscopy of the Earth's Atmosphere and Interstellar Medium in: K.N. Rao, A.Weber (Eds.)*. San Diego: Academic Press, 1992.

[55] Zhilinskii B.I., Perevalov V.I., Tyuterev Vl.G., *Method of Irreducible Tensorial Operators in the Theory of Molecular Spectra*. Novosibirsk: Nauka, 1987.

[56] Rey M., Nikitin A.V., Tyuterev Vl.G., Ab initio ro-vibrational Hamiltonian in irreducible tensor formalism: a method for computing energy levels from potential energy surfaces for symmetric-top molecules *Molec. Phys.* 2010;108: 2121-2135.

[57] Rey M., Nikitin A.V., Tyuterev V.G., Complete nuclear motion Hamiltonian in the irreducible normal mode tensor operator formalism for the methane molecule *J. Chem. Phys* 2012;136, no. 24: 244106.

[58] Lodi L. , Tennyson J., Line lists for H218O and H217O based on empirical line positions and ab initio intensities *J. Quant. Spectrosc. Radiat. Transfer.* 2012;113: 850–858.

[59] Tyuterev V.G., Kochanov R.V., Tashkun S.A., Accurate ab initio dipole moment surfaces of ozone: First principle intensity predictions for rotationally resolved spectra in a large range of overtone and combination bands *Journal of Chemical Physics* 2017;146: 064304.

[60] Nikitin A.V., Rey M., Tyuterev V.G., Accurate line intensities of methane from first-principles calculations *Journal of Quantitative Spectroscopy and Radiative Transfer* 2017;200: 90-99.

[61] Nikitin A.V., Rey M., Champion J.-P., Tyuterev Vl.G., Extension of the MIRS computer package for modeling of molecular spectra: from effective to full ab initio ro-vibrational hamiltonians in irreducible tensor form. *J. Quant. Spectrosc. Radiat. Transfer* 2012;113: 1034-1042.

[62] Nikitin A.V. IvanovaY.A., Rey M., Tashkun S.A., Toon G.C., Sung, K., Tyuterev Vl.G., Analysis of PH3 spectra in the Octad range 2733–3660 cm-1 *J. Quant. Spectrosc. Radiat. Transf.* 2017;203: 472-479.

[63] Maki A.G., Sams R.L., Olson W.B., Infrared Determination of Co for phosphine via perturbation-allowed 8(K — I) = ±3 Transitions in the 3v2 band. *J. Chem. Phys.* 1973;58: 4502–4512.

[64] Nikitin A.V. , Kochanov R.V.Visualization and identification of spectra by the SpectraPlot, Visualization and identification of spectra by the SpectraPlot program. *Atmos Ocean Opt* 2011;24: 931-941.

[65] Bouanich J.P., Walrand J., Blanquet G., N2-broadening coefficients in the ν2 and ν4 bands of PH3 *J.Mol. Spectrosc.* 2005;232: 40–46.

[66] Salem J., Bouanaich J.P., Walrand J., Aroui H., Blanquet G., Hydrogen line broadening in the v2 and v4 bands of phosphine at low temperature *J. Mol. Spectrosc.* 2004;228: 23–30.

[67] Sharpe S., Johnson T., Sams R., Chu P., Rhoderick G., Johnson P., Gas-phase databases for quantitative infrared spectroscopy. Appl. Spectrosc. *Appl. Spectrosc.* 2004;58: 1452 – 1461.

[68] Johnson T., Sams R., Sharpe S., The PNNL Quantitative Infrared Database for Gas-Phase Sensing: A spectral Library for Environmental, Hazmat, and Public Safety Standoff Detection. *Proceedings of SPIE - The International Society for Optical Engineering* 2004;5269: 159-169.

[69] Pacific Nortwest National Laboratory. [Online]. http://www.pnnl.gov